https://doi.org/10.1093/plphys/kiad473 PLANT PHYSIOLOGY 2024: 194: 137–152

Plant Physiology®

Research Article

Balanced callose and cellulose biosynthesis in Arabidopsis quorum-sensing signaling and pattern-triggered immunity

Xiaolin Liu [1,†] Zhiming Ma [1,†] Tuan Minh Tran [1,2,†] Carsten Rautengarten [3,4] Yingying Cheng,[5] Liang Yang [5,6] Berit Ebert [3,4] Staffan Persson [7,8,9] and Yansong Miao [1,*]

1 School of Biological Sciences, Nanyang Technological University, Singapore 637551, Singapore
2 Department of Biology, University of South Alabama, Mobile, AL 36688, USA
3 School of BioSciences, University of Melbourne, Parkville, Victoria 3010, Australia
4 Faculty of Biology and Biotechnology, Ruhr University Bochum, Bochum 44810, Germany
5 Singapore Centre for Environmental Life Sciences Engineering, Nanyang Technological University, Singapore 637551, Singapore
6 School of Medicine, Southern University of Science and Technology, Nanshan District, Shenzhen 518055, China
7 Department of Plant and Environmental Sciences (PLEN), University of Copenhagen, 1871 Frederiksberg C, Denmark
8 Copenhagen Plant Science Center, University of Copenhagen, 1871 Frederiksberg C, Denmark
9 Joint International Research Laboratory of Metabolic and Developmental Sciences, State Key Laboratory of Hybrid Rice, SJTU-University of Adelaide Joint Centre for Agriculture and Health, School of Life Sciences and Biotechnology, Shanghai Jiao Tong University, Shanghai 200240, China

*Author for correspondence: yansongm@ntu.edu.sg
†These authors contribute equally to this work.
The author responsible for distribution of materials integral to the findings presented in this article in accordance with the policy described in the Instructions for Authors (https://academic.oup.com/plphys/pages/General-Instructions) is Yansong Miao (Email: yansongm@ntu.edu.sg).

Abstract

The plant cell wall (CW) is one of the most important physical barriers that phytopathogens must conquer to invade their hosts. This barrier is a dynamic structure that responds to pathogen infection through a complex network of immune receptors, together with CW-synthesizing and CW-degrading enzymes. Callose deposition in the primary CW is a well-known physical response to pathogen infection. Notably, callose and cellulose biosynthesis share an initial substrate, UDP-glucose, which is the main load-bearing component of the CW. However, how these 2 critical biosynthetic processes are balanced during plant–pathogen interactions remains unclear. Here, using 2 different pathogen-derived molecules, bacterial flagellin (flg22) and the diffusible signal factor (DSF) produced by *Xanthomonas campestris* pv. *campestris*, we show a negative correlation between cellulose and callose biosynthesis in Arabidopsis (*Arabidopsis thaliana*). By quantifying the abundance of callose and cellulose under DSF or flg22 elicitation and characterizing the dynamics of the enzymes involved in the biosynthesis and degradation of these 2 polymers, we show that the balance of these 2 CW components is mediated by the activity of a β-1,3-glucanase (BG2). Our data demonstrate balanced cellulose and callose biosynthesis during plant immune responses.

Received June 23, 2023. Accepted July 18, 2023. Advance access publication August 30, 2023

Introduction

The plant cell wall (CW) is an essential physical frontier and the first obstacle encountered by pathogens during the interplay between pathogens and plants. The CW comprises cellulose microfibrils, hemicelluloses, pectins, other polymers (e.g. callose, lignin), and proteins, many of which are heavily glycosylated (Pedersen et al. 2023), depending on plant and tissue type. Dynamic remodeling of this framework occurs during plant–microbe interactions, which changes CW polymers' structure and composition (Bellincampi et al. 2014). Changes in CW production and the assembly of CW polymer-crosslinked scaffolds (nanoscale-to-mesoscale organization) modulate CW mechanical properties, such as yielding and elasticity, during physiological and pathological stimuli (Zhang et al. 2021). Upon host–pathogen communication, pathogenic microbes secrete CW-degrading enzymes to breach the CW for efficient infection (van Kan 2006, Choquer et al. 2007). Plants may respond to such breaches through recognition of pathogen-associated molecular patterns (PAMPs, plant senses pathogen-derived molecules) and the damage-associated molecular patterns (DAMPs, plant senses plant-derived molecules) to trigger host surveillance mechanisms (Nühse 2012, Davidsson et al. 2013).

The status of callose (β-1,3-glucan) is regulated through the coordination of callose synthases (CalSs) and β-1,3-glucanases (Kudlicka and Brown Jr 1997, Zavaliev et al. 2011). During plant development, callose is an essential component of cytokinesis progression (Thiele et al. 2009), plasmodesmata function (Zavaliev et al. 2011), pollen wall patterning (Nishikawa et al. 2005), phloem vascular development (Xie et al. 2011), and cell-to-cell signaling in the root meristem (Müller et al. 2015). Callose deposition between the plasma membrane (PM) and the existing CW is also a multifaceted defense response in plant hosts during pathogen infection (Luna et al. 2011), triggered, for example, by MAMP elicitation (e.g. bacterial flagellin epitope flg22, chitosan), filamentous fungal attack, and wounding (Gómez-Gómez et al. 1999, Jacobs et al. 2003, Schulze-Lefert 2004, Luna et al. 2011). Such callose accumulation contributes to disease resistance, e.g. against fungal infection (Ton and Mauch-Mani 2004). As such, CalS and degradation by β-1,3-glucanases are tightly regulated during host–pathogen communication. It has been reported that Arabidopsis (*Arabidopsis thaliana*) *β-1,3-GLUCANASE2* (*BG2*) (also termed *PATHOGENESIS-RELATED PROTEIN 2*, *PR2*), encoding a β-1,3-glucanase, is transcriptionally repressed by pathogen infection-induced abscisic acid accumulation, resulting in enhanced callose deposition (Oide et al. 2013). In addition, BG2 is also targeted by fungal effector proteins to suppress the plant host immune response (Bueno et al. 2022). Interestingly, callose shares its substrate, UDP-glucose (UDP-Glc), with that of cellulose (β-1,4-glucan) (Bulone et al. 1995, Somerville 2006, Bulone 2007). Crystalline cellulose, the load-bearing structure in the CW, is synthesized at the PM by cellulose synthase (CESA) complexes (Kroon-Batenburg and Kroon 1997, Lampugnani et al. 2019). Cellulose-deficient mutants show altered disease resistance due to CW changes (Ellis and Turner 2001, Hernandez-Blanco et al. 2007). These perturbations to CW tune hormone pathways and cause lignification, both of which contribute to host defense responses, at least in Arabidopsis (Ellis and Turner 2001, Caño-Delgado et al. 2003).

Cellulose, among other CW polymers, may engage with callose to form 3D polysaccharide networks in both Arabidopsis roots and synthetic cellulose–callose hydrogels (Abou-Saleh et al. 2018). Such associations were also observed, for example, in the pollen of tobacco (*Nicotiana tabacum*) under physiological conditions (Ferguson et al. 1998) or in Arabidopsis leaf CWs during fungal infection (Eggert et al. 2014). Notably, both CESAs and CalSs can be associated with detergent-resistant membrane (DRM) compartments (Verma and Hong 2001, Schrick et al. 2012, Srivastava et al. 2013), and their activities in DRM have been shown in vitro (Cifuentes et al. 2010). Incubation of UDP-Glc with the DRM extracts from tobacco BY-2 suspension cells led to the production of both cellulose and callose (Cifuentes et al. 2010). Interestingly, an antagonistic relationship between callose and cellulose biosynthesis was observed upon wounding, which leads to a noticeable increase in CalS but a decrease in CESA at the wound site as identified via immunolabeling (Nakashima et al. 2003). However, we still have limited knowledge about the mechanistic regulation of callose and cellulose polymers regarding both their physical association and coordinated biosynthesis during plant–pathogen communication.

Here, we show an interplay between cellulose and callose synthesis when plants encounter 2 types of bacterial virulence factors: the bacterial flagellin (flg22) (Boller and Felix 2009) and an emerging bacterial quorum-sensing (QS) molecule called diffusible signal factor (DSF) derived from *Xanthomonas campestris* pv. *campestris* (*Xcc*) (Newman et al. 2004, Chatterjee et al. 2008, Brock et al. 2010). DSF, structural formula as cis-11-methyl-2-dodecenoic acid, is a primary cell–cell communication signal of *Xcc*, which regulates the production of virulence factors and biofilm formation (Deng et al. 2011, He et al. 2023). Recently, DSF was found to regulate Arabidopsis immune responses by inducing the production of both phytosterol species and cellulose fibers (Tran et al. 2020, Ma et al. 2021). Here, we demonstrate that DSF regulates cellulose and callose biosynthesis in an antagonistic manner, in which cellulose synthesis was induced by DSF elicitation, while callose production was reduced through stimulation *BG2* expression. Interestingly, such an inverse association of callose and cellulose fiber production seems to be a general molecular mechanism to balance the 2 polymers in plant CWs. Using both pharmacological treatments and genetic tools, we showed that the inhibition of one polymer type results in an increase in the other. In addition, although flg22 does not directly increase cellulose production, *cesa* mutants showed enhanced deposition of callose during flg22-triggered pattern-triggered immunity (PTI) responses. Taken together, we demonstrated a mechanism by which callose and cellulose production is balanced

upon perceiving microbe molecular patterns during plant–bacteria interactions.

Results

DSF and bacterial flagellin differentially regulate the turnover of cellulose and callose in Arabidopsis

CWs, and in particular callose deposition, contribute to how plant cells are affected and respond to environmental challenges, including interactions with pathogens. Since callose and cellulose biosynthesis share the same substrate, we investigated how this process is coordinated upon exposure to pathogenic microbe-derived molecules. To elucidate the crosstalk between plant CW production and defense-related callose deposition during infection, we choose 2 bacteria-derived molecules that evidently alter CW composition: the PAMP-flagellin (here we used flg22 peptides), and the bacterial QS signal DSF, which is an emerging signaling molecule in plant defense and development (Götz et al. 2007, Schenk et al. 2014, Tran et al. 2020).

To gain further insight into how DSF and flg22 affect plant cellulose and callose biosynthesis/degradation pathways, we performed a transcriptomic analysis using 8-d-old Arabidopsis ecotype Columbia-0 (Col-0) wild-type (WT) seedlings pretreated with either 150 nM of flg22 or 20 μM of DSF, respectively. This RNA-Seq analysis revealed that 742 genes were differentially expressed (>2-fold) in DSF-treated seedlings, representing 2.7% of the coding sequences in the genome of the Arabidopsis accession Col-0 (Fig. 1, A and B). Gene Ontology (GO) analysis of DSF-reprogrammed gene expression revealed enrichment of several plant development-related and immune response-related pathways, such as "postembryonic root morphogenesis," "responses to salicylic acid," "response to insect," "response to bacterium," "response to reactive oxygen species," as well as the "beta-glucan metabolic process" (Fig. 1C). This outcome, in conjunction with our prior finding that DSF inhibits plant

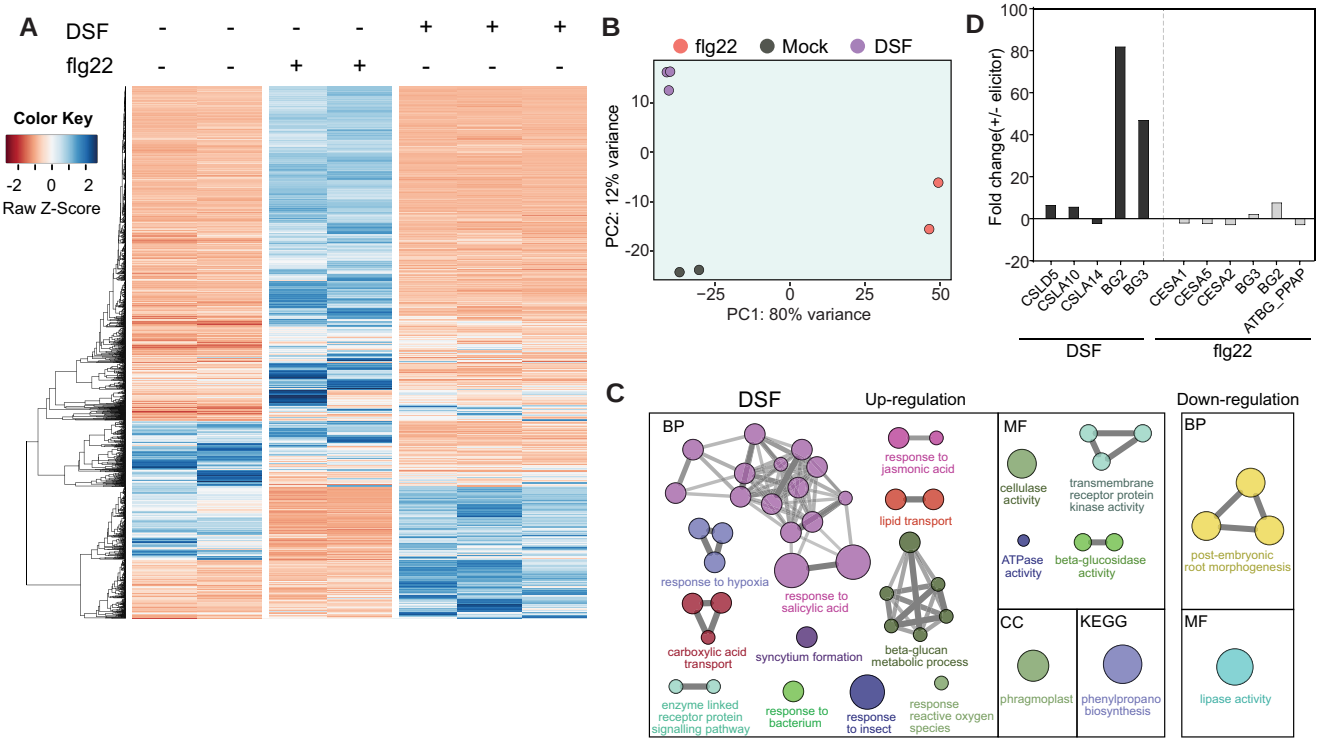

Figure 1. Transcriptome analysis of Arabidopsis under DSF- or flg22-elicitation. **A**) Heatmap of the overall transcriptomic profiles with hierarchical clustering generated by ggplot2. Z-score represents the standardization of gene expression as shown by the color key, indicating the downregulated- or upregulated-genes. Five-day-old seedlings were treated with 20 μM DSF or DMSO for 3 d and further subjected to an additional 2 h treatment in the absence (water) or presence of 150 nM flg22. Three samples, DMSO + water (termed Mock), DMSO + flg22 (termed flg22), and DSF + water (termed DSF), with their respective biological replicates ($n = 2$ for Mock and flg22, $n = 3$ for DSF), were collected, and the total RNA was extracted, and reverse transcribed for sequencing. **B)** Principal component analysis based on expression values showed separation of the transcriptomes into distinct treatment groups. **C)** GO analysis of the DSF elicitation-induced transcriptomic changes in Arabidopsis WT seedlings using Cytoscape with ClueGO plug-in. Differentially expressed genes with minimal 4-fold upregulated and 3-fold downregulated as compared to Mock control were extracted. Each node represents a GO term. Colors in connected groups represent key GO biological processes (BPs), cellular components (COs), molecular functions (MFs), or Kyoto Encyclopedia of Genes and Genomes (KEGG) pathways as indicated. **D)** Differentially expressed callose and cellulose biosynthesis/degradation-related genes in response to DSF or flg22 treatment from **A**). The gene expression data sets are summarized in **Supplemental Table S1**.

innate immune responses by altering membrane lipid composition (Tran et al. 2020), reveals a complex interaction among distinct plant immune response pathways in response to bacterial DSF signals.

Next, we performed a targeted search of this dataset to investigate the expression of genes encoding the enzymes that control the biosynthesis/degradation of cellulose and callose, including CESAs, CalSs, and β-1,3-glucanases. Remarkably, DSF treatment induced a major increase in gene expression of the β-1,3-glucanase *BG2* (pathogenesis-related protein 2, *PR-2*), as well as the *BG2* homolog *BG3* (Fig. 1D, Supplemental Table S1). In contrast, Arabidopsis showed a divergent transcript profile upon flg22 stimulation as compared to that of DSF-treated seedlings (Fig. 1D). Although callose deposition is a well-established response upon PAMP perception, flg22 elicitation did not show similar changes in the expression of genes encoding callose biosynthesis/degradation-relevant enzymes as in contrast to those detected upon DSF treatment (Fig. 1D, Supplemental Table S1), suggesting different regulatory mechanisms of CW polymers in response to flg22 and DSF. Besides *BG2* and *BG3*, also several *CESAs* or *CELLULOSE SYNTHASE-LIKE* (*CSL*) genes showed differential expression under either DSF or flg22 treatment (Fig. 1D, Supplemental Table S1). Nevertheless, those genes all have much lower basal expression compared to well-studied *CESAs* such as *CESA3* and *CESA6* (Hamann et al. 2004), which, however, were not among the differentially expressed genes. The above results suggested β-1,3-glucanases as the important targets underlying the flg22 and DSF signaling.

DSF regulates the balance of callose and cellulose by stimulating the expression of β-1,3-glucanase

To further validate the transcriptional changes of *BG2* induced by DSF treatment, we conducted reverse transcription quantitative PCR (RT-qPCR) and confirmed that *BG2* showed a drastic upregulation of approximately 400-fold compared to the control (Fig. 2A). Additionally, we investigated the protein levels of BG2 by generating a transgenic Arabidopsis line expressing BG2-GFP under the control of its native promoter (*pBG2::BG2-GFP*) (Fig. 2B). Consistent with the RNA-Seq and RT-qPCR results, we found an apparent increase in the abundance of BG2 protein in BG2-GFP seedlings treated with DSF (Fig. 2, C and D), whereas flg22 elicitation attenuated the BG2 protein abundance (Fig. 2, C and D). BG2 acts as β-1,3-glucanase/callase by hydrolyzing the β-1,3-glycosidic bonds of β-1,3-glucans (Oide et al. 2013, Zavaliev et al. 2013). Thus, we suspected that DSF treatment would directly reduce the CW callose accumulation, which was further examined through immunostaining.

Arabidopsis Col-0 seeds were directly germinated on the ½ MS agar for 3 d with or without 20 μM DSF before the seedlings were subjected to immunostaining with an anti–β-1,3-glucan antibody. Callose deposition was quantified and compared by measuring the mean intensity of the fluorescent signal of the anti–β-1,3-glucan antibody at the cell–cell junctions of the primary root (Supplemental Fig. S1A). Compared to untreated plants, roots of DSF-treated seedlings showed a noticeable decrease in anti–β-1,3-glucan signal intensity, indicating a reduction of callose deposition (Fig. 2E). Interestingly, the Arabidopsis *BG2* loss of function mutant, *bg2*, demonstrated an attenuated callose response to DSF, i.e. the DSF-induced callose reduction was largely abolished in the *bg2* (Fig. 2F), indicating that DSF causes a reduction in callose accumulation by inducing high BG2 callase expression.

We next measured the crystalline cellulose levels in Arabidopsis seedlings using the Updegraff method (Updegraff 1969) and observed that DSF treatment led to a robust elevation (~ 1.5-fold) of cellulose production, consistent with previous reports (Ma et al. 2021). However, the observed increase in cellulose production was significantly attenuated in the *bg2* mutant (Fig. 2G). As DSF elicitation did not apparently change the overall monosaccharide composition except for the glucose levels (Ma et al. 2021), we hypothesized that a switch from callose to cellulose biosynthesis occurred upon DSF elicitation, possibly through the BG2 callase activity. The UDP-Glc is the substrate for both CalSs and CESAs. Therefore, the levels of UDP-Glc could determine the synthesis rates of callose and cellulose (Amor et al. 1995). We thus assessed whether any changes to the nucleotide sugars pools occurred upon DSF treatment. To test this, we measured 11 nucleotide sugars, including UDP-Glc, by LC-MS/MS (Rautengarten et al. 2016). We did not observe any changes in UDP-Glc, as well as any other nucleotide sugars under DSF elicitation (Fig. 2H). These data confirm that the nucleotide sugar pools are robust against elevated BG2 activity caused by DSF treatment, similar to what has been observed that the UDP-Glc levels are relatively stable across the diurnal changes in WT Arabidopsis (Gibon et al. 2006, Ivakov et al. 2017).

We next applied a similar treatment on the *phosphoglucomutase* (*pgm*) mutant that has impaired sugar content and precursor pools of callose and cellulose in a diurnal changes-dependent manner (Gibon et al. 2006). PGM catalyzes the reversible interconversion between glucose-1-phosphate (G-1-P) and glucose-6-phosphate (G-6-P). We first observed visibly lower callose deposition in the roots of *pgm* mutant (Supplemental Fig. S1, B and C). Consistently, DSF-triggered upregulation of cellulose biosynthesis was also attenuated in *pgm* mutant (Supplemental Fig. S1D). While it is important to note that the *pgm* mutant also has altered the content of starch and soluble sugars during diurnal changes, our results suggest that changes to the sugar availability, and perhaps therefore also the UDP-Glc levels, could impair the biosynthesis of both the cellulose and callose. Although this hypothesis remains to be directly tested, it becomes clear that changes to carbon allocation impact the amplitude of the inverse association of cellulose and callose synthesis.

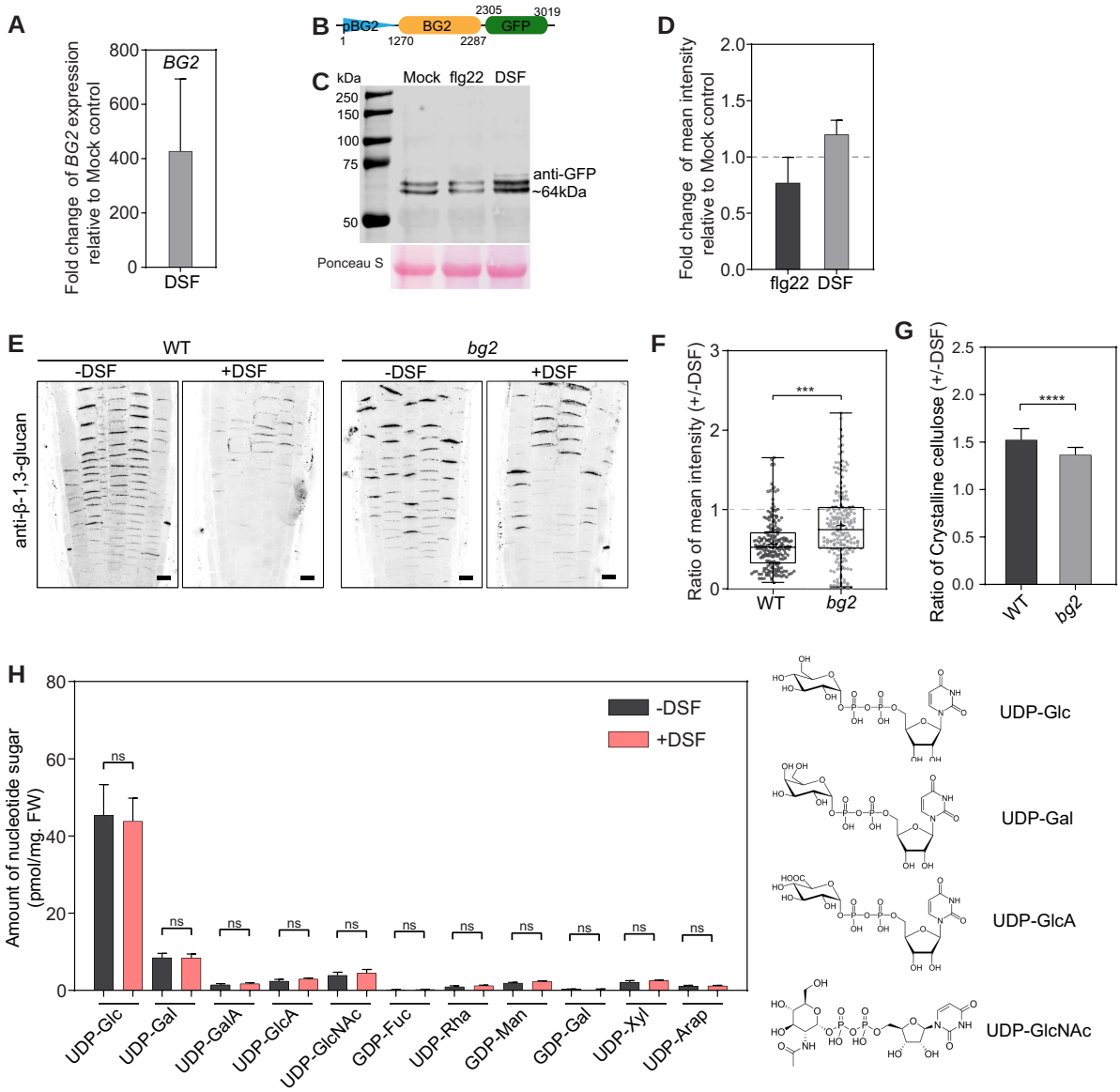

Figure 2. DSF regulates the callose and cellulose production in a reverse manner through β−1, 3-glucanase. **A**) Relative expression level of *BG2* (*At3g57260*) compared to Mock control analyzed by RT-qPCR analysis. Five-day-old seedlings were treated with 20 μM DSF for 3 d as in Fig. 1A. The error bar represents SD, $n = 6$ replicates from 2 biological repeats. **B)** Schematic illustration of the construction of *pBG2::BG2-GFP* in pGreen II backbone. The numbers indicate the relative positions of each element. **C)** Western blot of BG2-GFP detected with anti-GFP. Four-week-old leaves were cut into 4-mm discs, soaked in water containing DMSO or 20 μM DSF for 3 d and further treated without (water) or with 150 nM flg22 for 2 h. The resulting samples DMSO + water (Mock), DSF + water (DSF), and DMSO + flg22 (flg22) were collected. Then, the total proteins were extracted for western blot. Two bands at ∼ 64 kDa were recognized by anti-GFP, considering that BG2 might undergo posttranslation modification. Ponceau S-stained Rubisco large subunit was used as loading control. **D)** Quantification of BG2-GFP expression by analyzing the anti-GFP–detected signal intensity in **C**). Data were shown as ratios normalized to Mock samples. Gray dash line indicates the relative signal intensity in Mock samples. The error bar represents SD, $n = 3$ biological repeats. **E)** Representative images of immunostaining by anti–β-1,3-glucan in WT and *bg2* seedlings, which were directly germinated in ½ MS medium supplemented with or without 20 μM DSF for 3 d. Scale bars, 10 μm. **F)** Ratios of anti–β-1,3-glucan-immunostained signal intensity in DSF-treated samples **E**) compared to the mean value of the samples without DSF treatment. Gray dash line indicates the relative mean intensities of anti–β-1,3-glucan-immunostained signal in WT or *bg2* without DSF treatment. $n > 180$ data points (see Supplemental Fig. S1A) from at least 4 seedlings. **G)** Ratios of crystalline cellulose content in DSF-treated WT or *bg2* seedlings compared to the mean value of the samples without DSF treatment. Five-day-old WT or *bg2* seedlings were transferred to new ½ MS medium supplemented with or without 20 μM DSF for additional 3 d, and then the AIRs were extracted for crystalline cellulose measurement. The rrror bar represents SD, $n = 12$ replicates from 2 biological repeats. **H)** Quantitative analysis of the nucleotide sugar pools in 5-d-old WT seedlings treated with or without 20 μM DSF for additional 3 d. For LC-MS/MS measurements, nucleotide sugars were extracted and enriched as described in Rautengarten et al. 2016. The error bars represent SD, $n = 5$ biological replicates. Significant differences were determined via Student's *t*-test, assuming equal variances in **F**) and **G**) (****$P < 0.0001$, ***$P < 0.001$, ns = not significant).

A negative association between callose and cellulose fiber production

Given the aforementioned specific inverse association between callose and cellulose synthesis upon DSF elicitation, our results suggest that stimulating/inhibiting the biosynthesis of one polymer might reduce/increase the production of another that shares a common substrate. We examined this hypothesis by monitoring callose deposition and distribution using immunohistochemistry when reducing cellulose production using cellulose biosynthesis inhibitors. WT seedlings were treated with 2,6-dichlorobenzonitrile (DCB) or isoxaben (ISX) for 3 d prior to immunofluorescence staining using an anti−1,3-glucan antibody. DCB stalls the movement of the CESA complex at the PM (Tateno et al. 2016), and ISX depletes the CESAs from the PM (Brabham et al. 2014). Untreated plants showed a relatively homogenous distribution of β-1,3-glucan labeling in WT Arabidopsis roots, whereas CESA-inhibiting drugs, DCB and ISX, induced a noticeable increase in β-1,3-glucan signals in WT Arabidopsis roots (Fig. 3, A to C). The intensity of β-1,3-glucan labeling was mainly associated with transverse CWs in DCB or ISX treated—compared to untreated—WT Arabidopsis seedling roots, indicating a general increase in callose production (Fig. 3A). In line with this result, by adding ISX, a higher callose signal was also detected in DSF-treated WT seedlings (Fig. 3, D and E).

We next sought to further test our hypothesis in a reverse manner by examining the cellulose production while inhibiting the callose deposition. Here, we first utilized an Arabidopsis transgenic line constitutively overexpressing *BG2* (Oide et al. 2013). We found that the overexpression of *BG2* uniformly reduced the overall abundance of the β-1,3-glucan signal (Fig. 3, A to C), suggesting an effective callose degradation activity of BG2. This result is also consistent with the above results that DSF elicitation reduces the callose deposition by upregulating *BG2* expression (Fig. 2). Next, we measured the crystalline cellulose content, representing the cellulose biosynthesis rate, in the *BG2*-overexpression Arabidopsis seedlings. Five-day-old seedlings of WT and 35S-BG2 were treated with 0.5 nM ISX or 1 nM DCB for 3 d, and then the alcohol insoluble residues (AIRs) were extracted for crystalline cellulose measurement using the anthrone hydrolysis method (Updegraff 1969, Lei et al. 2015). As expected, compared to WT, 35S-BG2 showed a significant ∼1.5-fold increase in cellulose content under control conditions (mock), which was reduced by coincubation with either ISX or DCB (Fig. 3F).

To further validate that callose degradation could enhance the cellulose biosynthesis rate, we also measured crystalline cellulose content in Arabidopsis seedlings treated directly with commercial β-1,3-glucanase for 3 d. By applying this enzyme, a dose-dependent efficacy in reducing callose production was observed through immunohistochemistry (Supplemental Fig. S2, A to C). Starting from 0.5 mg/mL, β-1,3-glucanase treatment on Arabidopsis seedlings already displayed a significant reduction in overall β-1,3-glucan immunofluorescence intensity (Supplemental Fig. S2, A to C). We then measured the crystalline cellulose content in Arabidopsis seedlings treated with the same doses of β-1,3-glucanase. As expected, β-1,3-glucanase-treated plants displayed significant increases in crystalline cellulose in a β-1,3-glucanase dose-dependent manner (Fig. 3G), demonstrating the link between callose degradation and cellulose synthesis. The biosynthesis of cellulose drives the movement of CESAs along the cortical microtubules, which has been extensively documented through live-cell imaging of fluorescently tagged CESAs (Paredez et al. 2006). We, therefore, also quantified cellulose fiber synthesis by measuring the density and mobility of fluorescence-labeled CESA complexes in Arabidopsis seedlings expressing *pCESA6::tdTomato-CESA6* in the presence or absence of a β-1,3-glucanase. Here, the fluorescence density of CESA puncta indicates the number of CESA complexes per area unit, whereas puncta speed represents the active production of cellulose fibers (Paredez et al. 2006, Bringmann et al. 2012). tdTomato-CESA6 seedlings were imaged by Variable Angle-Total Internal Reflection Fluorescence Microscopy in the midhypocotyl region of etiolated Arabidopsis that were treated with β-1,3-glucanases for 24 h. We did not observe a significant change in CESA density at the PM (Supplemental Fig. S2, D and E). However, the CESA puncta speed increased significantly from 154 ± 79 (mean ± SD) nm/min in untreated seedlings to 176 ± 90 nm/min and 217 ± 94 nm/min in the seedlings treated with 2and 5 mg/mL β-1,3-glucanase, respectively (Fig. 3, H and I). Together, these results indicate that a negative association between callose and cellulose fiber production exists in plant CW synthesis.

Antagonistic regulation of callose deposition and cellulose synthesis inhibition in PTI response

Enhanced callose deposition is one of the well-documented PTI responses after PAMP elicitation (Clay et al. 2009). We next compared callose deposition in Arabidopsis WT and the CESA mutants at the locus of *CESA3* (*je5*) or *CESA6* (*prc1-1*), which showed reduced cellulose production (Desprez et al. 2007, Rui and Anderson 2016) in aniline blue staining experiments. Here, we analyzed leaf cells to measure callose deposition as root cells reportedly show weaker and spatially restricted PAMP-trigged immune responses (Beck et al. 2014, Emonet et al. 2021). flg22 induced an apparent enhancement of callose deposition after 24 h, which could be abolished by overexpression of the BG2 callase (Fig. 4A), whereas no detectable change in crystalline cellulose content was observed (Ma et al. 2021). This result suggests different regulatory mechanisms for PTI and DSF signaling, particularly regarding the regulation of cellulose and callose production. Nevertheless, we observed that both *je5* and *prc1-1* seedlings showed enhancement of the aniline blue signals compared to WT seedlings after elicitation with 1 μM flg22 (Fig. 4, A and B), indicating increased callose

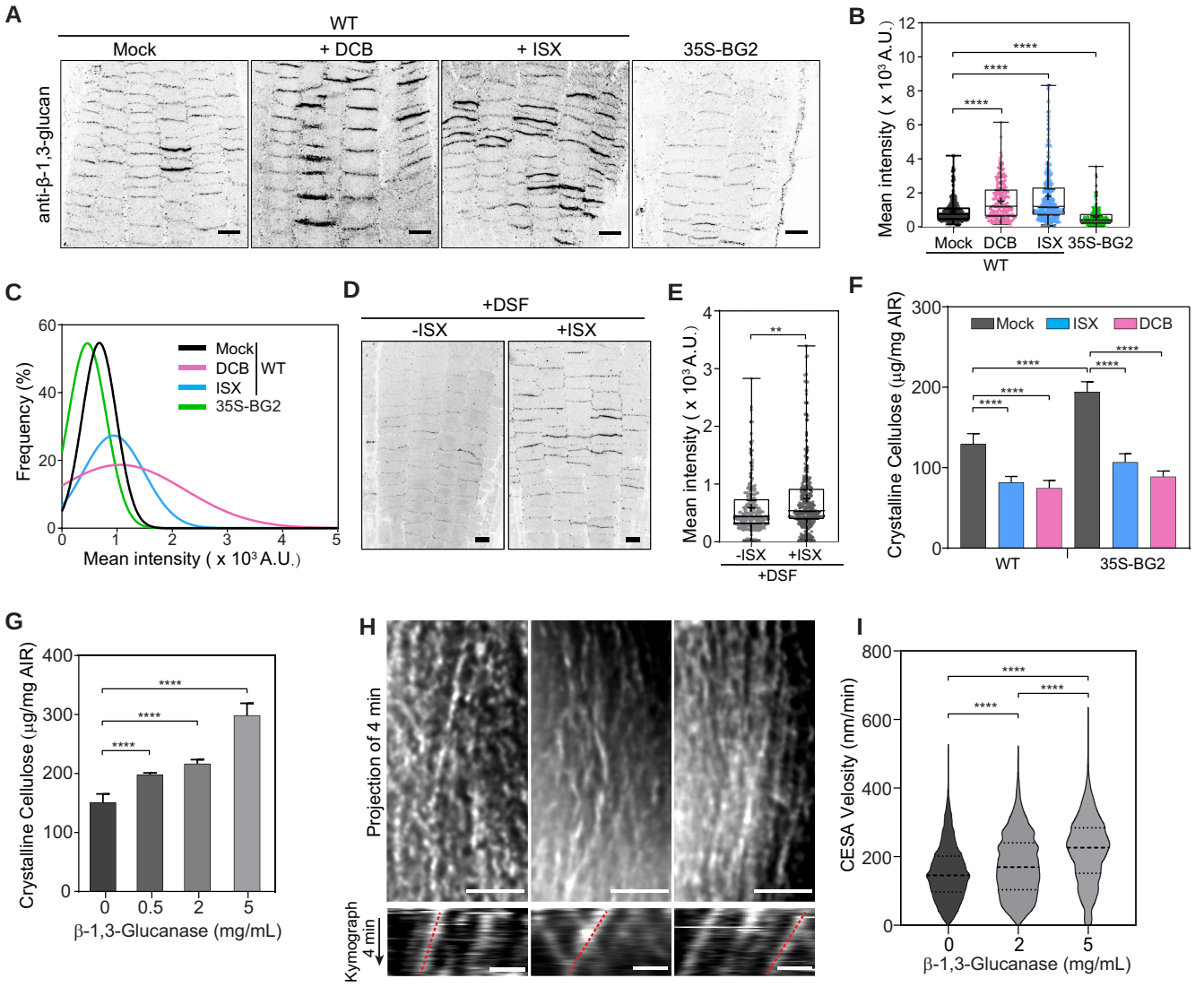

Figure 3. Balance of callose and cellulose biosynthesis in Arabidopsis at steady states. **A**) Representative images of immunostaining by anti−β-1,3-glucan in 35S-BG2 or WT seedlings treated with or without DCB or ISX. Seeds were directly germinated in ½ MS medium supplemented with or without 1 nM DCB or 0.5 nM ISX as indicated for 3 d. Scale bars, 10 μm. **B**) Quantification of anti−β-1,3-glucan-immunostained signal intensity (arbitrary unit, A.U.) in CW as in **A**). $n = 200$ data points from 5 seedlings. **C)** The frequency distribution of the anti−β-1, 3-glucan-immunostained signal intensity in **B**), fitted by Gaussian distribution. **D)** Representative images of immunostaining by anti−β-1, 3-glucan in WT seedlings treated by DSF with or without ISX coinoculation. Seeds were germinated on ½ MS agar supplemented with 20 μM DSF with or without 0.5 nM ISX coinoculation for 2.5 d. Scale bars, 10 μm. **E)** Quantification of anti−β-1,3-glucan-immunostained signal intensity in CW as in **D**). $n = 240$ data points from 5 seedlings. **F)** Crystalline cellulose content in 5-d-old WT and 35S-BG2 seedlings treated with or without 1 nM DCB or 0.5 nM ISX for additional 3 d, followed by AIRs extraction for crystalline cellulose measurement. The error bar represents SD, $n = 12$ replicates from 2 biological repeats. **G)** Crystalline cellulose content of 5-d-old WT seedlings treated with 0, 0.1, 0.5, 2.0, and 5.0 mg/mL of β-1,3-glucanase for additional 3 d before AIR extraction for crystalline cellulose measurement. The error bar represents SD, $n = 6$ replicates from 2 biological repeats. **H)** The time projections of trajectories (upper panel) and kymograph (lower panel) of tdT-CESA6 particles. Time projections were generated by average intensity of 49 frames collected at 5 s interval. Representative kymographs show the moving trajectory (highlighted by red lines) of tdT-CESA6 particles within 4 min duration. Scale bars, 5 μm in upper panel and 1 μm in lower panel, respectively. **I)** Quantitative analysis of tdT-CESA6 moving velocity on the PM in **H**). Data were shown as violin plot indicating the 25% and 75% quartiles (dot dash lines) and median (dash line). $n > 1{,}300$ tracks from 5 seedlings in each condition. Significant differences were determined via Student's *t*-test, assuming equal variances in **E**) or 1-way ANOVA with multiple comparisons in **B**), **F**), **G**), and **I**) (**$P < 0.01$, ****$P < 0.0001$, ns = not significant).

production in the cellulose biosynthesis mutants during PTI signaling. Notably, flg22 elicitation did not apparently change the abundance of cellulose/callose synthesis/degradation-related enzymes (Fig. 1, A and C). Our results suggest that additional mechanisms may exist that regulate the activities of enzymes involved in cellulose/callose turnover and that those may cause callose enrichment in cellulose-deficient conditions.

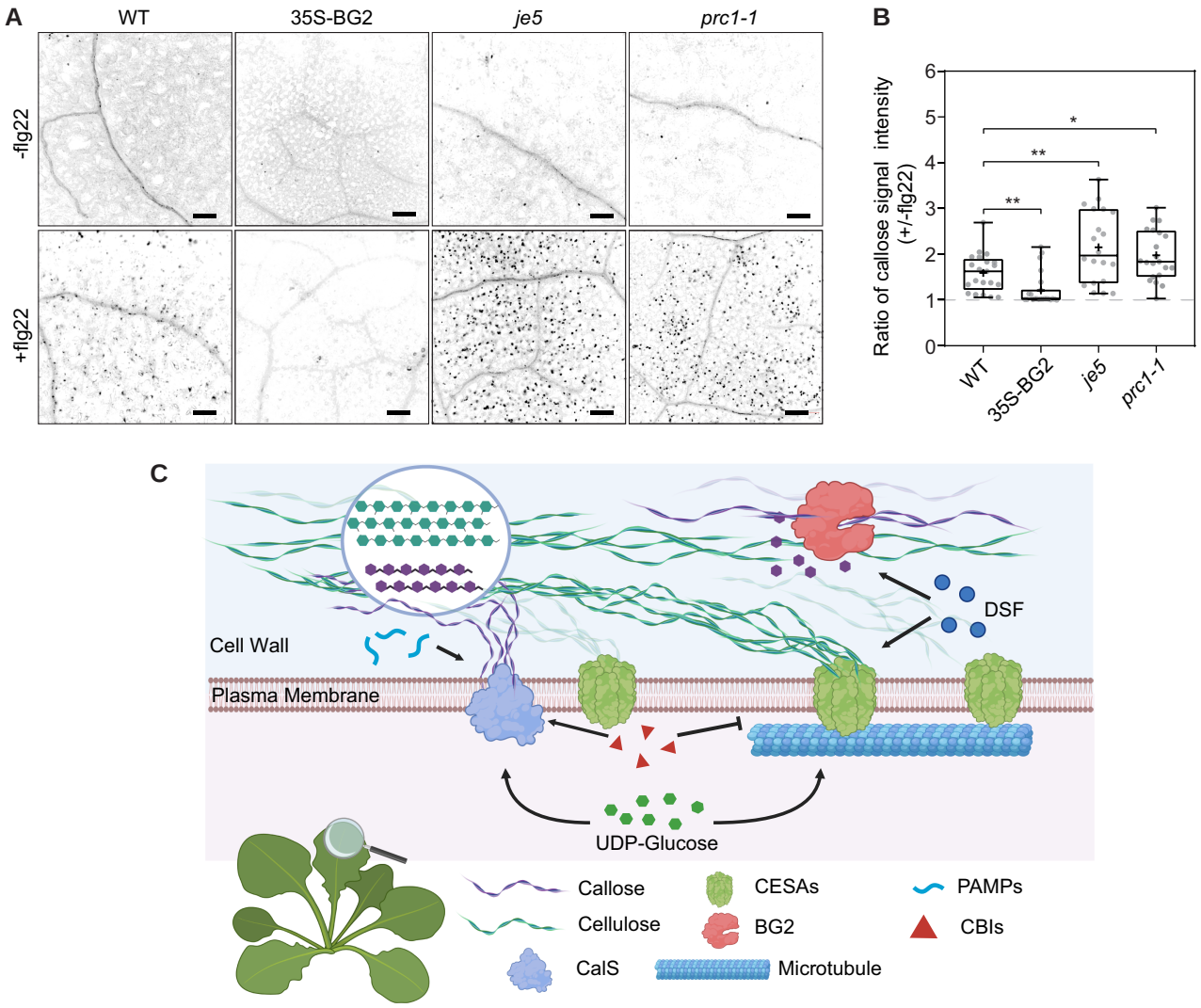

Figure 4. Cellulose biosynthesis mutants demonstrated enhanced flg22-triggered callose deposition. **A**) Representative images of aniline blue stained callose deposition on leaf epidermal cells. Two-week-old seedlings of WT, 35S-BG2, *je5*, and *prc1-1* were treated with or without 1 μM flg22 for 24 h. Scale bar, 100 μm. **B)** Ratios of callose production as stained by aniline blue in flg22-treated seedlings compared to the mean value of the samples without flg22 treatment as in **A**). Gray dash line indicates the relative mean values of callose signal in the samples without flg22 treatment. $n > 20$ biological replicates from 6 seedlings. Significant differences were determined via 1-way ANOVA with multiple comparisons (**$P < 0.01$, *$P < 0.05$). **C)** The proposed working model for balanced callose and cellulose biosynthesis under immune signaling. The callose deposition is tuned by CalS and BG2, while cellulose biosynthesis is mediated by CESA. By sharing the same UDP-Glc as the common biosynthesis substrate, callose and cellulose are antagonistic regulated under the elicitation of bacteria-derived molecules: DSF and PAMP-flg22. DSF hijacks PRRs and suppresses the flg22-triggered immunity responses, including callose production in response to flg22 (Tran et al. 2020). DSF upregulates the cellulose biosynthesis, evidenced by the enhanced CESA velocity (Ma et al. 2021), and downregulates the callose deposition mediated by BG2 expression (this study). However, flg22 induces callose deposition without positive effects on cellulose biosynthesis (Ma et al. 2021). Cellulose biosynthesis inhibition (CBI) increases the callose deposition elicited by flg22, and BG2 overexpression reduces flg22-induced callose deposition. Arrows and blunt arrows represent positive and negative regulations, respectively. Image was created with BioRender.com.

PAMP-induced apoplastic reactive oxygen species (ROS) bursts are responsible for callose deposition during defense signaling (Daudi et al. 2012, Smith and Heese 2014). In line with that, we observed that the Arabidopsis mutant *rbohd*, which is defective in RESPIRATORY BURST OXIDASE HOMOLOG D (RBOHD), demonstrated a reduction in callose deposition after flg22 elicitation compared to WT plants (Supplemental Fig. S3, A and B). We next asked whether *je5* or *prc1-1*'s ROS production is a contributing factor to the changes in callose deposition observed during PTI signaling. However, both *je5* and *prc1-1* showed decreased levels of ROS induction by flg22 elicitation (Supplemental Fig. S3C), demonstrating that ROS was unlikely the reason for the callose deposition in cellulose-deficient mutants.

Discussion

CW remodeling during DSF signaling

The CW is the load-bearing structure and structural barrier of plant cells, in which the different polysaccharides vary depending on environmental conditions and signal transductions. The biosynthesizing and degrading enzymes, the physical interactions of different polysaccharides, and the extensibility and relaxation of the plant CWs are fundamental factors for CW biology (Cosgrove 2015, Lampugnani et al. 2018). CW polymers are dynamically assembled to support specific mechanical needs during morphology and stress adaptation, such as pathogenic invasion. It is becoming increasingly clear that CW remodeling is one of the essential plant defense mechanisms (Jacobs et al. 2003, Liu et al. 2014, Huang et al. 2019, Dora et al. 2022). While CW polymers and their corresponding processing enzymes have been well documented, the underlying mechanisms of CW remodeling during plant immune responses are complex and poorly understood.

Microbial pathogens transmit a variety of signaling biomolecules, such as PAMPs (e.g. flagellin, EF-Tu, lipopolysaccharides, chitin, etc.) or chemical small molecule-QS signals, which could be perceived by plant hosts that dramatically affect plant development or modulate immune responses (Kutschera et al. 2019, Tran et al. 2020). There is mounting evidence that bacterial QS molecules are capable of modulating plant development and defense mechanisms. N-acylhomoserine lactones (AHLs) secreted from Gram-negative bacteria are the best-studied QS molecule, of which impact has been studied in plants. Long-chain AHLs (C12 to C14) from root-colonizing microbes in the rhizosphere are effectively perceived by plants and modulate host responses, such as the AHL effect in priming plant defense by activating mitogen-activated protein kinase (MAPK) cascades (Schikora et al. 2011, Schenk et al. 2014). Similarly, a medium-chain 3-hydroxy fatty acid (mc-3-OH-FA)-type QS molecule was reported to stimulate plant PTI responses through receptor kinase LIPOOLIGOSACCHARIDE-SPECIFIC REDUCED ELICITATION (LORE) (Kutschera et al. 2019). However, more recently, *Xanthomonas* DSF species were shown to promote disease in both *Citrus paradisi Macfadyen* and Arabidopsis, in which DSF represses plant defense responses, although some defense-relevant genes are upregulated at very high DSF concentrations (Kakkar et al. 2015, Li et al. 2019, Tran et al. 2020). The distinct plant responses to different QS molecules are most likely the result of diverse recognition mechanisms of bacterial QS signals evolved in the plant host, perhaps through the presence of receptors or metabolizing enzymes. *Xanthomonas* DSF induces phytosterol production, attenuating PTI responses in Arabidopsis (Tran et al. 2020).

Interestingly, in this study, we found an additional response to DSF in remodeling Arabidopsis root CWs. DSF antagonistically regulates cellulose and callose biosynthesis and drastically upregulates the callose degrading enzyme, BG2/PR2. The striking inverse regulation of cellulose and callose biosynthesis during DSF treatment is mediated by enhanced β-1,3-glucanase activity and less likely via fine-tuning of the *CESA* gene expression (Fig. 1D) or the restriction of the shared substrate, UDP-Glc (Figs. 2H and 4C). The underlying mechanisms of the induction of cellulose fiber biosynthesis through DSF and the interplays between the enzymes for cellulose and callose synthesis are worth future studies. An investigation of potential crosstalk between cellulose and phytosterol biosynthesis pathways or a quantitative analysis of the cellulose and phytosterol at spatial resolution in cell and tissue scale, which are lacked in this study, might reveal additional insight. DSF directly regulates Arabidopsis defense responses by increasing phytosterol production (Tran et al. 2020). Arabidopsis sterol mutants have reduced bulk cellulose biosynthesis but not in pectin and neutral sugar biosynthesis (Schrick et al. 2004). Both CESAs and CalSs might be localized in lipid nanodomains at the PM (Somerville 2006, Schrick et al. 2012, Takahashi et al. 2013), which may be targeted by both host- and pathogen-derived molecules during plant–microbe interactions (Jaillais and Ott 2020, Ma et al. 2022, Tran et al. 2022). Although DSF did not affect the CESA density at the PM (Ma et al. 2021), whether DSF-mediated lipid changes and sterol enhancement would influence the activity of CESA and CalS remains elusive and requires further studies.

ROS, callose, and cellulose production during immune responses

CW biosynthesis and modification should be closely linked during plant immune response and feedback control. The bidirectional communication between pathogens and plants are constantly evolving and are, therefore, divergent under different conditions of host–pathogen communication (Dora et al. 2022). Upon bacterial infection, plant immune responses are directly activated by bacterial-derived PAMPs. Rapid ROS production and subsequent callose deposition are hallmarks of PTI responses that in return cause remodeling of CW and, thereby, plant pathogenesis (Engelsdorf et al. 2018). The compositional and mechanical changes of plant CW scaffolds enhance the defense through different approaches, including the production of plant-derived DAMPs, mechanical control of plasmodesmata aperture, and ROS production (Jacobs et al. 2003, Nühse 2012, Oide et al. 2013). However, little is known about how ROS affects the downstream polymerization of callose, cellulose, or other polysaccharides. ROS burst by PAMP elicitation was significantly attenuated in Arabidopsis mutants deficient in cellulose biosynthesis (isoxaben-treated or mutation at ISOXABEN RESISTANT1 locus, *irx1-6*) or xylan acetylation (mutation at ESKIMO1, *esk1*, or at the locus encoding beta subunit of the G protein complex, *abg1-2*) (Denness et al. 2011, Escudero et al. 2017). Here, we also demonstrated direct manipulation of flg22-triggered ROS production in cellulose biosynthesis mutants (Supplemental Fig. S3C). Earlier DSF was shown to reduce flg22-stimulated

ROS production by impairing the clustering and activation of pattern recognition receptors (PRRs) (Tran et al. 2020). The negative regulation of the ROS bursts by DSF is unlikely derived from reduced cellulose content because DSF can upregulate cellulose biosynthesis. In addition, DSF also impaired ROS production. For the same reason, ROS is unlikely to be the intermediate regulator of DSF-triggered cellulose biosynthesis.

In summary, our findings illustrate a sophisticated process that maintains the structural integrity of the CW through a balanced biosynthesis of callose and cellulose. This balance can be influenced by 2 potential pathways: defense response signaling or feedback regulation emanating from the dynamic interaction between callose and cellulose when CW integrity is compromised (Figs. 3 and 4C). Under conditions with limited sucrose, the reverse correlation between callose and cellulose was disrupted (Hamann et al. 2009). This process could also be mediated by stress conditions affecting CW integrity, irrespective of the substrate limitation (Engelsdorf et al. 2018). Future research explores whether the reciprocal biosynthesis of callose–cellulose persists in CW damage-sensing mutants could help to determine whether the stress signaling pathway or substrate allocation contributes to the biosynthesis of callose or cellulose, and whether these 2 mechanisms operate independently. In addition, the perturbation of CW integrity during DSF exposure mediated through enhanced cellulose biosynthesis (Ma et al. 2021) and callose degradation (via *BG2* upregulation, this study) could originate from changes to the molecular framework required for the precise function of cellulose and CalSs. Among those factors, both formin-mediated actin assembly and PM compositions are significantly altered during DSF signaling (Tran et al. 2020, Ma et al. 2021). Besides the CW-PM-actin cytoskeleton continuum (Fig. 4C), it is of special interest for future investigations whether additional players may contribute to the DSF/PTI signaling, such as direct participation of phytosterol substrates in cellulose biosynthesis or integrity sensing of wall-associated kinase sensors (Engelsdorf et al. 2018).

Materials and methods

Plant materials and growth conditions

Arabidopsis (*A. thaliana*) Columbia accession (Col-0) was used in this study. tdT-CESA6 (Sampathkumar et al. 2013), 35S-BG2 (originally termed as *35S::PR2pad3*) (Oide et al. 2013), *je5* (Desprez et al. 2007), *prc1-1* (Fagard et al. 2000), and *pgm* (Usadel et al. 2008) were reported in previous studies. *bg2* (Salk_20950 °C) and *rbohd* (Salk_035391C) were obtained from ABRC (The Ohio State University). To generate the BG2-GFP transgenic line, the native promoter and cDNA fragment of *BG2* (At3g57260) were synthesized (Synbio Tech, USA) and fused with the pGreen II binary vector backbone (Hellens et al. 2000) to generate the *pBG2::BG2-GFP* construct, which was then transformed to *Agrobacterium tumefaciens* strain AGL-1. Transformation of Col-o WT seedlings was further conducted via the floral dip method (Clough and Bent 1998). Transgenic seeds selection was performed in ½ MS medium containing 10 mg/L glufosinate ammonium.

Arabidopsis seeds were surface-sterilized in 15% bleach (v/v) for 5 min and rinsed with sterilized distilled water for 3 times. After stratification at 4 °C in dark for a minimum of 2 d, the seeds were germinated on ½ MS media containing: 0.22% (w/v) MS basal salts (Phytotech lab), 1% (w/v) sucrose, 0.05% (w/v) MES, pH5.8, and 0.8% (w/v) agar. Unless specific note, the seedlings were grown in growth chambers (Panasonic MLR-352H-PE) under long-day conditions (16 h light and 8 h dark cycle) under 22 °C.

tdTomato-CESA6 image and analysis

The tdT-CESA6 seeds were directly germinated on ½ MS media in dark, and the middle regions of 3- to 4-d-old etiolated hypocotyl were imaged via the Zeiss Elyra PS.1 platform equipped with variable angle total internal reflection fluorescence (VA-TIRF) illumination though a 100×, NA 1.46 oil objective. The tdTomato signal was excited at 561 nm with 24 W/cm^2 of laser intensity, and the emission was collected at 570 to 650 nm through a sCMOS camera (PCO-edge) with 5 s interval. TIRF angle (~62° used) was adjusted until getting the best signal to noise ratio. The time-lapse images of tdT-CESA6 were deconvolved using Huygens Essential (SVI) by setting the deconvolution parameters as signal noise ratio = 20, iteration = 30, and quality threshold = 0.01. To quantify the tdT-CESA6 particle dynamics, the deconvoluted images were first cropped into ROIs avoiding the background signal beyond the hypocotyl cell region. tdT-CESA6 particle tracking was then performed cropped ROIs using the plugin-Trackmate (Tinevez et al. 2017) in Fiji (NIH, USA). The estimated particle diameter was set to 0.4 μm for particle detection. To track the particle trajectories, the linking max distance, gap-closing max distance, and gap-closing max frame gap were set to 0.2, 0.2, and 2 μm, respectively. Trajectories with more than 25 frames were subjected to quantification of particle moving velocity by dividing the tracking distance with the duration time. The final particle velocity was confirmed by manually checking the kymograph. The particle density of tdT-CESA6 was analyzed using particles in the first frame of the deconvoluted image by dividing the resulting particle total count with the area of ROI. The final particle selection was confirmed by comparison with the original image.

Crystalline cellulose analysis

To prepare the AIR samples, 4-d-old seedlings were transferred to ½ MS plate supplemented with indicated drugs for an additional 3 d. Seedlings were firstly frozen in liquid nitrogen and homogenized using PowerLyzer 24 Homogenizer (Qiagen). The tissue powder was then rinsed sequentially by 70%, 80%, and 100% ethanol and centrifuged at 13,000 × *g* for 10 min to pellet the CW extraction, which was further

incubated with 1:1 (v/v) methanol:chloroform mixture for 2 h. After centrifugation at 13,000 × *g* for 10 min, the pellet was washed in acetone completely and air-dried overnight. Subsequently, the destarch step was performed by incubating the pellet with α-amylase overnight under 50 °C. The measurement of crystalline cellulose content was conducted through the Updegraff method (Updegraff 1969). Briefly, 1 mL of acetic nitric reagent was incubated with AIR samples for 30 min at 121 °C. The pellets were then collected by centrifugation at 13,000 × *g* for 10 min and washed with 1 mL acetone. After centrifugation and air-drying, 200 μL 72% sulfuric acid was added for another 1 h of incubation. After which 800 μL pure water was added and mixed well. For final measurement, 500 μL of the above mixture was taken out, mixed with 1 mL of ice-cold 0.2% (w/v) anthrone solution and then incubated at 98 °C for 10 min and cooled down to room temperature. The OD_{620} of the solution was further measured in a Biotek Cytation 5 cell imaging multimode reader (Agilent Technologies).

Aniline blue staining of callose

Two-week-old seedlings were fixed and detained in 1:3 (v/v) acetic acid/ethanol mixture until leaves were transparent, followed by washing in 150 mM K_2HPO_4 for 20 min and repeating 3 times. The seedlings were then stained for at least 3 h by 0.01% (w/v) aniline blue dissolved in 150 mM K_2HPO_4 in a 6-well plate covered by aluminum foil. After staining, samples were embedded in 50% glycerol before imaging. The callose signal was captured using Zeiss LSM 780 confocal laser scanning microscopy equipped with an Alpha Plan Apochromat 10× objective with an excitation at 405 nm and emission collection at 420∼470 nm.

ROS measurement

Arabidopsis plants were grown for 1 mo in short-day conditions (8 h light and 16 h dark cycle) under 22 °C. Leaf discs with a diameter of 5 mm were punched and cut into 5 leaf stripes, which were transferred into a 96-well microtiter plate filled with 200 μL of distilled H_2O in each well and incubated overnight for relieving the wounding response. To induce detective ROS production, the water was removed, and 200 μL of prechilled elicitation solution was added with a final concentration of 20 ng/mL peroxidase (Sigma-Aldrich), 34 μg/mL luminol (Sigma-Aldrich), and 1 μM flg22 (synthesized by GL Biochem). Immediately, the luminescence was monitored using BioTek Cytation 5 cell imaging multimode reader (Agilent Technologies) for 40 min with 1 min of time interval. To analyze the data, the luminescence signal reading against time was plotted in Prism 7.0 (GraphPad). Area under the curve was calculated to indicate the total ROS production.

Western blot

Four-week-old Arabidopsis seedlings grown in short-day conditions (8 h light and 16 h dark cycle) under 22 °C were prepared for western blot to detect the BG2 protein production. Six leaf discs with a diameter of 4 mm were transferred to a 6-well microtiter plate and incubated in liquid ½ MS media supplied without (DMSO) or with 20 μM of DSF for 3 d and then subjected to an additional 2 h of treatment in the absence (water) or presence of 150 nM flg22. The resulting samples DMSO + water (Mock), DSF + water (DSF), and DMSO + flg22 (flg22) were collected. To obtain total protein extraction, leaf discs were frozen in liquid nitrogen and ground and then lysed in 200 μL extraction buffer (100 mM Tris-HCl pH 8.0, 250 mM sucrose, 15 mM EDTA, 5% [v/v] glycerol, 0.5% [w/v] PVP K25, 25 mM sodium fluoride, 50 mM sodium pyrophosphate, 1 mM sodium molybdate, pierce protease inhibitor [Thermo Fisher, 1 tablet/50 mL], 1 mM PMSF, 3 mM DTT). After centrifugation at 20,000 × *g* for 15 min, the supernatant fraction was collected and loaded in a 10% SDS-PAGE gel. After separation, proteins were transferred into a 0.2 μm nitrocellulose membrane. BG2-GFP was probed with rabbit monoclonal antibody against GFP (Torrey Pines BioLabs, 1:200 dilution, overnight at 4 °C) and detected by incubating with IRDye 800CW Goat anti-Rabbit IgG secondary antibody (LI-COR, 1:2000 dilution, 1 to 2 h at room temperature). Ponceau S-stained signal of Rubisco was used as loading control.

Immunostaining of β-1,3-glucan

Three-day-old seedlings of WT as well as mutants were fixed in 4% (w/v) paraformaldehyde for 1 h in a vacuum desiccator. Samples were successively rinsed 3 times with PBS and incubated with 2% (w/v) Driselase (Sigma-Aldrich) for 60 min at 37 °C for CW digestion. The membrane permeabilization was conducted with 3% (v/v) IGEPAL (Sigma-Aldrich) in PBS containing 0.1% (v/v) Triton X-100% and 10% (v/v) DMSO. After blocking with 3% (w/v) BSA in PBS for 1 h, the seedlings were incubated with mouse monoclonal antibody against β-1,3-glucan (BioSupplies) at a dilution of 1:200. Secondary antibody goat antimouse IgG Alexa Fluor Plus 488 (Invitrogen) was added at a 1:2000 dilution following the washing steps with PBS. The signal was then imaged immediately under Zeiss LSM 780 confocal laser scanning microscopy following the complete wash, the Alexa 488 signal was excited at 488 nm with 36 μW of laser intensity, and the emission was collected at 495 to 575 nm.

β-1,3-Glucanase treatment

For VA-TIRF imaging of hypocotyls with β-1,3-glucanase treatment, the tdT-CESA6 seeds were germinated on ½ MS plate for 2.5 d in the dark and treated with β-1,3-glucanase (Sigma-Aldrich) for an additional 24 h. The middle part of hypocotyl was imaged through VA-TIRF. For crystalline cellulose measurement with β-1,3-glucanase treatment, the 5-d-old WT seedlings were treated with 0, 0.1, 0.5, 2.0, and 5.0 mg/mL of β-1,3-glucanase for additional 3 d, and then the AIRs were extracted for crystalline cellulose measurement.

Nucleotide sugar extraction for LC-MS/MS measurement

The nucleotide extraction was done as described previously (Rautengarten et al. 2019). Briefly, 8-d-old seedlings were homogenized in liquid nitrogen using a mortar and pestle. Six hundred microliters of ice-cold chloroform/methanol (3:7) solution was added, and the sample was vortexed for 5 s. The solution was stored at −20 °C for 2 h, and then 400 μL of ice-cold water was added and mixed thoroughly for 5 s using a vortex mixer. After centrifugation at 20,000 × *g* for 5 min at 4 °C, the upper aqueous phase was collected into a 15 mL tube, which was further washed 2 more times by adding 400 μL ice-cold water, centrifuging, and pooling. Further, 2.5 mL ice-cold water was added to the 15 mL tube prior to lyophilization of the sample overnight. One microliter of 10 mM ammonium bicarbonate was added to the dried sample, mixed, and briefly spun down. Equilibration of an EnviCarb SPE (Sigma-Aldrich) was performed using 3 mL of 80% acetonitrile with 0.1% trifluoroacetic acid (TFA) followed by 2 mL of water. The sample in 10 mM ammonium bicarbonate was added to the SPE column, and the column washed with 2 mL of water and then 2 mL of 25% acetonitrile and finally 2 mL of 50 mM triethylamine/acetic acid (TEAA) pH 7.0. Elution was undertaken using 2 mL of 25% acetonitrile with 50 mM TEAA pH 7.0. After a lyophilization step overnight, the nucleotide sugars were resuspended in 200 μL of ice-cold water and analyzed by LC-MS/MS. LC-MS/MS was performed using porous graphitic carbon as the stationary phase on an 1100 series HPLC system (Agilent Technologies) and a 4000 QTRAP LC/MS/MS system (SCIEX) equipped with a TurboIonSpray ion source using methods previously described (Rautengarten et al. 2014).

RNA-Seq and data analysis

Five-day-old Arabidopsis seedlings were transferred to new ½ MS plates containing 20 μM DSF or DMSO for additional 3 d and then were further treated without (water) or with 150 nM flg22 for 2 h. The resulting samples DMSO + water (Mock), DSF + water (DSF), and DMSO + flg22 (flg22) were collected for RNA-seq analysis. Plant tissue was frozen in liquid nitrogen and kept at −80 °C. RNA extraction was performed using RNeasy Plant Minikit (Qiagen) according to the manufacturer instruction. Each treatment includes 2 to 3 biological replicates.

Arabidopsis full genome sequence was downloaded from Ensembl Genomes in CLC Genomics Workbench 8.0 (Qiagen) as reference and annotated by The Arabidopsis Information Resource (TAIR) from GO Consortium (https://geneontology.org/docs/download-ontology/). RNA-seq raw data were imported into CLC Genomics Workbench 8.0 (Qiagen) to obtain reads of each gene by "RNA-Seq Analysis" application. Comparison of expression level was performed by DESeq2 package in RStudio 3.3.1 with a negative binomial test (adjusted *P*-value <0.05). Heat map was generated by heatmap.plust package. Principal component analysis plot was generated by ggplot2 package.

RT-qPCR validation

Turbo DNase (Ambion) and RNAClean XP kit (Agencourt) were used for DNase treatment and repeated twice. Qubit Fluorometer (Thermo Fisher) was applied for the evaluation of the quality of RNA samples. cDNA was synthesized using oligo-d(T) primer on the SuperScript III First-Strand Synthesis system. RT-qPCR was conducted using Kapa SYBR FAST qPCR Master mix with primers specific PR2 (Xiao and Chye 2011), with EF-1α gene used as the internal control for calibration of all samples (Czechowski et al. 2005). The data were collected by Applied Biosystem StepOnePlus RealTime PCR system (Applied Biosystem) and analyzed using the manufacturer's software. Each was performed in triplicates.

Statistical analysis

Statistical analyzes were performed in Prism 7.0 (GraphPad). Comparisons between 2 groups were conducted using 2-tailed Student's *t*-test assuming equal variances, while the multiple comparisons between 3 or more groups were carried out using 1-way ANOVA with multiple comparisons: $^{*}P < 0.05$, $^{**}P < 0.01$, $^{***}P < 0.001$, $^{****}P < 0.0001$, ns means no "significant difference." Final data were plotted as bar graphs (mean + SD) or box plots showing the 25% and 75% quartiles with median inside the mean value (indicated as "+"). The cartoon in Fig. 4C was created with BioRender.com.

Accession numbers

The original RNA-Seq data of this article can be found in the NCBI Bioproject under accession numbers PRJNA504740 (https://www.ncbi.nlm.nih.gov/bioproject/?term=PRJNA504740). Accession numbers of the major genes reported in this study are listed as follows: *BG2*, AT3G57260; *BG3*, AT5G57240; *CESA3*, AT5G05170; *CESA6*, AT5G64740; and *RBOHD*, AT5G47910.

Acknowledgments

We thank Christina Dixelius (Swedish University of Agricultural Sciences, Sweden) for sharing the 35S-BG2 Arabidopsis seeds. We thank Lay Yin Tang and Alma Turšić-Wunder for helping in RNA sample preparation for RNAseq analysis. We thank Daniela Moses, Yap Zhei Hwee, and Rikky Wenang Purbojati for technical assistance in the RNA-Seq experiment. We thank Xiaoming Pu for performing the validation of homozygote screening of *rbohD*.

Author contributions

X.L. and Y.M. conceived and designed the study. X.L. performed most of the plant-based experiments. Z.M. constructed the *pBG2::BG2-GFP* in pGreen II and validated the homozygote screening of *bg2*. T.M.T. performed RNA extraction and RT-qPCR validation. Y.C. helped transcriptome profiling and data analysis. C.R. performed the UDP-sugar measurements. C.R. and B.E. analyzed the data. S.P. shared the *je5*, *prc1-1*, tdT-CESA6 Arabidopsis seeds and provided valuable intellectual input to the story. X.L. Z.M. T.M.T. and Y.M. wrote the manuscript with feedback from all authors. Y.M. supervised the studies.

Supplemental data

The following materials are available in the online version of this article.

Supplemental Table S1. Transcript fold change of the selected genes in Fig. 1D.

Supplemental Figure S1. Restricted callose and cellulose synthesis in PGM mutant.

Supplemental Figure S2. β-1,3-Glucanase treatment effectively reduced β-1,3-glucan abundance in Arabidopsis root tissue.

Supplemental Figure S3. Attenuated ROS production in mutants of cellulose biosynthesis.

Funding

This study was supported by Singapore Ministry of Education (MOE) Tier 1 (RG32/20 and RT11/20) and Tier 2 (MOE-T2EP30122-0021) to Y.M. in Singapore. C.R. acknowledges the financial aid of an Albert Shimmins COVID-19 support fund. B.E. acknowledges ARC Future Fellowship (FT160100276), Discovery Grant (DP180102630) Awards, and support from the University of Melbourne Botany Foundation. S.P. thanks a Villum, 2 Novo Nordisk Foundation, Danish National Research Foundation, and grants (25915, 19OC0056076, 20OC0060564, and DNRF155, respectively).

Conflict of interest statement. The authors declare no conflict of interests.

Data Availability

The original RNA-Seq data of this article can be found in the NCBI Bioproject under accession numbers PRJNA504740. Other data is available upon request.

References

Abou-Saleh RH, Hernandez-Gomez MC, Amsbury S, Paniagua C, Bourdon M, Miyashima S, Helariutta Y, Fuller M, Budtova T, Connell SD, et al. Interactions between callose and cellulose revealed through the analysis of biopolymer mixtures. Nat Commun. 2018:**9**(1):4538. https://doi.org/10.1038/s41467-018-06820-y

Amor Y, Haigler CH, Johnson S, Wainscott M, Delmer DP. A membrane-associated form of sucrose synthase and its potential role in synthesis of cellulose and callose in plants. Proc Natl Acad Sci USA. 1995:**92**(20):9353–9357. https://doi.org/10.1073/pnas.92.20.9353

Beck M, Wyrsch I, Strutt J, Wimalasekera R, Webb A, Boller T, Robatzek S. Expression patterns of flagellin sensing 2 map to bacterial entry sites in plant shoots and roots. J Exp Bot. 2014:**65**(22):6487–6498. https://doi.org/10.1093/jxb/eru366

Bellincampi D, Cervone F, Lionetti V. Plant cell wall dynamics and wall-related susceptibility in plant–pathogen interactions. Front Plant Sci. 2014:**5**:228. https://doi.org/10.3389/fpls.2014.00228

Boller T, Felix G. A renaissance of elicitors: perception of microbe-associated molecular patterns and danger signals by pattern-recognition receptors. Annu Rev Plant Biol. 2009:**60**(1):379–406. https://doi.org/10.1146/annurev.arplant.57.032905.105346

Brabham C, Lei L, Gu Y, Stork J, Barrett M, Debolt S. Indaziflam herbicidal action: a potent cellulose biosynthesis inhibitor. Plant Physiol. 2014:**166**(3):1177–1185. https://doi.org/10.1104/pp.114.241950

Bringmann M, Li E, Sampathkumar A, Kocabek T, Hauser M-T, Persson S. POM-POM2/cellulose synthase interacting1 is essential for the functional association of cellulose synthase and microtubules in *Arabidopsis*. Plant Cell. 2012:**24**(1):163–177. https://doi.org/10.1105/tpc.111.093575

Brock AK, Willmann R, Kolb D, Grefen L, Lajunen HM, Bethke G, Lee J, Nürnberger T, Gust AA. The *Arabidopsis* mitogen-activated protein kinase phosphatase PP2C5 affects seed germination, stomatal aperture, and abscisic acid-inducible gene expression. Plant Physiol. 2010:**153**(3):1098–1111. https://doi.org/10.1104/pp.110.156109

Bueno TV, Fontes PP, Abe VY, Utiyama AS, Senra RL, Oliveira LS, Brombini Dos Santos A, Ferreira EGC, Darben LM, De Oliveira AB, et al. A phakopsora pachyrhizi effector suppresses PAMP-triggered immunity and interacts with a soybean glucan endo-1,3-β-glucosidase to promote virulence. Mol Plant Microbe Interact. 2022:**35**(9):779–790. https://doi.org/10.1094/MPMI-12-21-0301-R

Bulone V. In vitro synthesis and analysis of plant (1→ 3)-β-D-glucans and cellulose: a key step towards the characterization of glucan synthases. Cellulose: molecular and structural biology, 2007:123–145. https://doi.org/10.1007/978-1-4020-5380-1_8

Bulone V, Fincher GB, Stone BA. In vitro synthesis of a microfibrillar (1→3)-β-glucan by a ryegrass (*Lolium multiflorum*) endosperm (1→3)-β-glucan synthase enriched by product entrapment. Plant J. 1995:**8**(2):213–225. https://doi.org/10.1046/j.1365-313X.1995.08020213.x

Caño-Delgado A, Penfield S, Smith C, Catley M, Bevan M. Reduced cellulose synthesis invokes lignification and defense responses in *Arabidopsis thaliana*. Plant J. 2003:**34**(3):351–362. https://doi.org/10.1046/j.1365-313X.2003.01729.x

Chatterjee S, Wistrom C, Lindow SE. A cell–cell signaling sensor is required for virulence and insect transmission of *Xylella fastidiosa*. Proc Natl Acad Sci USA. 2008:**105**(7):2670–2675. https://doi.org/10.1073/pnas.0712236105

Choquer M, Fournier E, Kunz C, Levis C, Pradier J-M, Simon A, Viaud M. *Botrytis cinerea* virulence factors: new insights into a necrotrophic and polyphageous pathogen. FEMS Microbiol Lett. 2007:**277**(1):1–10. https://doi.org/10.1111/j.1574-6968.2007.00930.x

Cifuentes C, Bulone V, Emons AMC. Biosynthesis of callose and cellulose by detergent extracts of tobacco cell membranes and quantification of the polymers synthesized *in vitro*. J Integr Plant Biol. 2010:**52**(2):221–233. https://doi.org/10.1111/j.1744-7909.2010.00919.x

Clay NK, Adio AM, Denoux C, Jander G, Ausubel FM. Glucosinolate metabolites required for an Arabidopsis innate immune response.

Science. 2009:**323**(5910):95–101. https://doi.org/10.1126/science.1164627

Clough SJ, Bent AF. Floral dip: a simplified method for Agrobacterium-mediated transformation of *Arabidopsis thaliana*. Plant J. 1998:**16**(6):735–743. https://doi.org/10.1046/j.1365-313x.1998.00343.x

Cosgrove DJ. Plant expansins: diversity and interactions with plant cell walls. Curr Opin Plant Biol. 2015:**25**:162–172. https://doi.org/10.1016/j.pbi.2015.05.014

Czechowski T, Stitt M, Altmann T, Udvardi MK, Scheible W-R. Genome-wide identification and testing of superior reference genes for transcript normalization in *Arabidopsis*. Plant Physiol. 2005:**139**(1):5–17. https://doi.org/10.1104/pp.105.063743

Daudi A, Cheng Z, O'brien JA, Mammarella N, Khan S, Ausubel FM, Bolwell GP. The apoplastic oxidative burst peroxidase in *Arabidopsis* is a major component of pattern-triggered immunity. Plant Cell. 2012:**24**(1):275–287. https://doi.org/10.1105/tpc.111.093039

Davidsson P, Kariola T, Niemi O, Palva T. Pathogenicity of and plant immunity to soft rot pectobacteria. Front Plant Sci. 2013:**4**:191. https://doi.org/10.3389/fpls.2013.00191

Deng Y, Wu JE, Tao F, Zhang L-H. Listening to a new language: dSF-based quorum sensing in gram-negative bacteria. Chem Rev. 2011:**111**(1):160–173. https://doi.org/10.1021/cr100354f

Denness L, Mckenna JF, Segonzac C, Wormit A, Madhou P, Bennett M, Mansfield J, Zipfel C, Hamann T. Cell wall damage-induced lignin biosynthesis is regulated by a reactive oxygen Species- and jasmonic acid-dependent process in Arabidopsis. Plant Physiol. 2011:**156**(3):1364–1374. https://doi.org/10.1104/pp.111.175737

Desprez T, Juraniec M, Crowell EF, Jouy H, Pochylova Z, Parcy F, Höfte H, Gonneau M, Vernhettes S. Organization of cellulose synthase complexes involved in primary cell wall synthesis in *Arabidopsis thaliana*. Proc Natl Acad Sci USA. 2007:**104**(39):15572–-15577. https://doi.org/10.1073/pnas.0706569104

Dora S, Terrett OM, Sánchez-Rodríguez C. Plant–microbe interactions in the apoplast: communication at the plant cell wall. Plant Cell. 2022:**34**(5):1532–1550. https://doi.org/10.1093/plcell/koac040

Eggert D, Naumann M, Reimer R, Voigt CA. Nanoscale glucan polymer network causes pathogen resistance. Sci Rep. 2014:**4**(1):4159. https://doi.org/10.1038/srep04159

Ellis C, Turner JG. The Arabidopsis mutant cev1 has constitutively active jasmonate and ethylene signal pathways and enhanced resistance to pathogens. Plant Cell. 2001:**13**(5):1025–1033. https://doi.org/10.1105/tpc.13.5.1025

Emonet A, Zhou F, Vacheron J, Heiman CM, Dénervaud Tendon V, Ma KW, Schulze-Lefert P, Keel C, Geldner N. Spatially restricted immune responses are required for maintaining root meristematic activity upon detection of bacteria. Curr Biol. 2021:**31**(5):1012–1028.e7. https://doi.org/10.1016/j.cub.2020.12.048

Engelsdorf T, Gigli-Bisceglia N, Veerabagu M, Mckenna JF, Vaahtera L, Augstein F, Van Der Does D, Zipfel C, Hamann T. The plant cell wall integrity maintenance and immune signaling systems cooperate to control stress responses in *Arabidopsis thaliana*. Sci Signal. 2018:**11**(536):eaao3070. https://doi.org/10.1126/scisignal.aao3070

Escudero V, Jordá L, Sopeña-Torres S, Mélida H, Miedes E, Muñoz-Barrios A, Swami S, Alexander D, Mckee LS, Sánchez-Vallet A, et al. Alteration of cell wall xylan acetylation triggers defense responses that counterbalance the immune deficiencies of plants impaired in the β-subunit of the heterotrimeric G-protein. Plant J. 2017:**92**(3):386–399. https://doi.org/10.1111/tpj.13660

Fagard M, Desnos T, Desprez T, Goubet F, Refregier G, Mouille G, Mccann M, Rayon C, Vernhettes S, Höfte H. PROCUSTE1 encodes a cellulose synthase required for normal cell elongation specifically in roots and dark-grown hypocotyls of *Arabidopsis*. Plant Cell. 2000:**12**(12):2409–2423. https://doi.org/10.1105/tpc.12.12.2409

Ferguson C, Teeri T, Siika-Aho M, Read S, Bacic A. Location of cellulose and callose in pollen tubes and grains of *Nicotiana tabacum*. Planta. 1998:**206**(3):452–460. https://doi.org/10.1007/s004250050421

Gibon Y, Usadel B, Blaesing OE, Kamlage B, Hoehne M, Trethewey R, Stitt M. Integration of metabolite with transcript and enzyme activity profiling during diurnal cycles in Arabidopsisrosettes. Genome Biol. 2006:**7**(8):R76. https://doi.org/10.1186/gb-2006-7-8-r76

Gómez-Gómez L, Felix G, Boller T. A single locus determines sensitivity to bacterial flagellin in *Arabidopsis thaliana*. Plant J. 1999:**18**(3):277–284. https://doi.org/10.1046/j.1365-313X.1999.00451.x

Götz C, Fekete A, Gebefuegi I, Forczek ST, Fuksová K, Li X, Englmann M, Gryndler M, Hartmann A, Matucha M, et al. Uptake, degradation and chiral discrimination of N-acyl-D/L-homoserine lactones by barley (*Hordeum vulgare*) and yam bean (*Pachyrhizus erosus*) plants. Anal Bioanal Chem. 2007:**389**(5):1447–1457. https://doi.org/10.1007/s00216-007-1579-2

Hamann T, Bennett M, Mansfield J, Somerville C. Identification of cell-wall stress as a hexose-dependent and osmosensitive regulator of plant responses. Plant J. 2009:**57**(6):1015–1026. https://doi.org/10.1111/j.1365-313X.2008.03744.x

Hamann T, Osborne E, Youngs HL, Misson J, Nussaume L, Somerville C. Global expression analysis of CESA and CSL genes in Arabidopsis. Cellulose. 2004:**11**(3/4):279–286. https://doi.org/10.1023/B:CELL.0000046340.99925.57

He YW, Deng Y, Miao Y, Chatterjee S, Tran TM, Tian J, Lindow S. DSF-family quorum sensing signal-mediated intraspecies, interspecies, and inter-kingdom communication. Trends Microbiol. 2023:**31**(1):36–50. https://doi.org/10.1016/j.tim.2022.07.006

Hellens RP, Edwards EA, Leyland NR, Bean S, Mullineaux PM. Pgreen: a versatile and flexible binary Ti vector for Agrobacterium-mediated plant transformation. Plant Mol Biol. 2000:**42**(6):819–832. https://doi.org/10.1023/A:1006496308160

Hernandez-Blanco C, Feng DX, Hu J, Sanchez-Vallet A, Deslandes L, Llorente F, Berrocal-Lobo M, Keller H, Barlet X, Sanchez-Rodriguez C, et al. Impairment of cellulose synthases required for Arabidopsis secondary cell wall formation enhances disease resistance. Plant Cell. 2007:**19**(3):890–903. https://doi.org/10.1105/tpc.106.048058

Huang D, Sun Y, Ma Z, Ke M, Cui Y, Chen Z, Chen C, Ji C, Tran TM, Yang L, et al. Salicylic acid-mediated plasmodesmal closure via remorin-dependent lipid organization. Proc Natl Acad Sci USA. 2019:**116**(42):21274–21284. https://doi.org/10.1073/pnas.1911892116

Ivakov A, Flis A, Apelt F, Fünfgeld M, Scherer U, Stitt M, Kragler F, Vissenberg K, Persson S, Suslov D. Cellulose synthesis and cell expansion are regulated by different mechanisms in growing Arabidopsis hypocotyls. Plant Cell. 2017:**29**(6):1305–1315. https://doi.org/10.1105/tpc.16.00782

Jacobs AK, Lipka V, Burton RA, Panstruga R, Strizhov N, Schulze-Lefert P, Fincher GB. An Arabidopsis callose synthase, GSL5, is required for wound and papillary callose formation. Plant Cell. 2003:**15**(11):2503–2513. https://doi.org/10.1105/tpc.016097

Jaillais Y, Ott T. The nanoscale organization of the plasma membrane and its importance in signaling: a proteolipid perspective. Plant Physiol. 2020:**182**(4):1682–1696. https://doi.org/10.1104/pp.19.01349

Kakkar A, Nizampatnam NR, Kondreddy A, Pradhan BB, Chatterjee S. *Xanthomonas campestris* cell-cell signalling molecule DSF (diffusible signal factor) elicits innate immunity in plants and is suppressed by the exopolysaccharide xanthan. J Exp Bot. 2015:**66**(21):6697–6714. https://doi.org/10.1093/jxb/erv377

Kroon-Batenburg L, Kroon J. The crystal and molecular structures of cellulose I and II. Glycoconj J. 1997:**14**(5):677–690. https://doi.org/10.1023/A:1018509231331

Kudlicka K, Brown Jr RM. Cellulose and callose biosynthesis in higher plants (I. Solubilization and separation of (1->3)- and (1->4)-β-glucan synthase activities from mung bean). Plant Physiol. 1997:**115**(2):643–656. https://doi.org/10.1104/pp.115.2.643

Kutschera A, Dawid C, Gisch N, Schmid C, Raasch L, Gerster T, Schäffer M, Smakowska-Luzan E, Belkhadir Y, Vlot AC. Bacterial medium-chain 3-hydroxy fatty acid metabolites trigger immunity

in *Arabidopsis* plants. Science. 2019:**364**(6436):178–181. https://doi.org/10.1126/science.aau1279

Lampugnani ER, Flores-Sandoval E, Tan QW, Mutwil M, Bowman JL, Persson S. Cellulose synthesis–central components and their evolutionary relationships. Trends Plant Sci. 2019:**24**(5):402–412. https://doi.org/10.1016/j.tplants.2019.02.011

Lampugnani ER, Khan GA, Somssich M, Persson S. Building a plant cell wall at a glance. J Cell Sci. 2018:**131**(2):jcs207373. https://doi.org/10.1242/jcs.207373

Lei L, Singh A, Bashline L, Li S, Yingling YG, Gu Y. CELLULOSE SYNTHASE INTERACTIVE1 is required for fast recycling of cellulose synthase complexes to the plasma membrane in *Arabidopsis*. Plant Cell. 2015:**27**(10):2926–2940. https://doi.org/10.1105/tpc.15.00442

Li L, Li J, Zhang Y, Wang N. Diffusible signal factor (DSF)-mediated quorum sensing modulates expression of diverse traits in *Xanthomonas citri* and responses of citrus plants to promote disease. BMC Genomics. 2019:**20**(1):55. https://doi.org/10.1186/s12864-018-5384-4

Liu X, Grabherr HM, Willmann R, Kolb D, Brunner F, Bertsche U, Kühner D, Franz-Wachtel M, Amin B, Felix G, et al. Host-induced bacterial cell wall decomposition mediates pattern-triggered immunity in Arabidopsis. Elife. 2014:**3**:e01990. https://doi.org/10.7554/eLife.01990

Luna E, Pastor V, Robert J, Flors V, Mauch-Mani B, Ton J. Callose deposition: a multifaceted plant defense response. Mol Plant Microbe Interact. 2011:**24**(2):183–193. https://doi.org/10.1094/MPMI-07-10-0149

Ma Z, Liu X, Nath S, Sun H, Tran TM, Yang L, Mayor S, Miao Y. Formin nano-clustering mediated actin assembly during plant flagellin and DSF- signalings. Cell Rep. 2021:**34**(13):108884. https://doi.org/10.1016/j.celrep.2021.108884

Ma Z, Sun Y, Zhu X, Yang L, Chen X, Miao Y. Membrane nanodomains modulate formin condensation for actin remodeling in Arabidopsis innate immune responses. Plant Cell. 2022:**34**(1):374–394. https://doi.org/10.1093/plcell/koab261

Müller J, Toev T, Heisters M, Teller J, Moore KL, Hause G, Dinesh DC, Bürstenbinder K, Abel S. Iron-dependent callose deposition adjusts root meristem maintenance to phosphate availability. Dev Cell. 2015:**33**(2):216–230. https://doi.org/10.1016/j.devcel.2015.02.007

Nakashima J, Laosinchai W, Cui X, Malcolm Brown RM. New insight into the mechanism of cellulose and callose biosynthesis: proteases may regulate callose biosynthesis upon wounding. Cellulose. 2003:**10**(4):369–389. https://doi.org/10.1023/A:1027336605479

Newman KL, Almeida RP, Purcell AH, Lindow SE. Cell-cell signaling controls *Xylella fastidiosa* interactions with both insects and plants. Proc Natl Acad Sci USA. 2004:**101**(6):1737–1742. https://doi.org/10.1073/pnas.0308399100

Nishikawa S-I, Zinkl GM, Swanson RJ, Maruyama D, Preuss D. Callose (beta-1,3 glucan) is essential for Arabidopsis pollen wall patterning, but not tube growth. BMC Plant Biol. 2005:**5**(1):22. https://doi.org/10.1186/1471-2229-5-22

Nühse T. Cell wall integrity signaling and innate immunity in plants. Front Plant Sci. 2012:**3**:280. https://doi.org/10.3389/fpls.2012.00280

Oide S, Bejai S, Staal J, Guan N, Kaliff M, Dixelius C. A novel role of PR2 in abscisic acid (ABA) mediated, pathogen-induced callose deposition in *Arabidopsis thaliana*. New Phytol. 2013:**200**(4):1187–1199. https://doi.org/10.1111/nph.12436

Paredez AR, Somerville CR, Ehrhardt DW. Visualization of cellulose synthase demonstrates functional association with microtubules. Science. 2006:**312**(5779):1491–1495. https://doi.org/10.1126/science.1126551

Pedersen GB, Blaschek L, Frandsen KEH, Noack LC, Persson S. Cellulose synthesis in land plants. Mol Plant. 2023:**16**(1):206–231. https://doi.org/10.1016/j.molp.2022.12.015

Rautengarten C, Ebert B, Liu L, Stonebloom S, Smith-Moritz AM, Pauly M, Orellana A, Scheller HV, Heazlewood JL. The Arabidopsis Golgi-localized GDP-L-fucose transporter is required for plant development. Nat Commun. 2016:**7**(1):12119. https://doi.org/10.1038/ncomms12119

Rautengarten C, Ebert B, Moreno I, Temple H, Herter T, Link B, Doñas-Cofré D, Moreno A, Saéz-Aguayo S, Blanco F, et al. The Golgi localized bifunctional UDP-rhamnose/UDP-galactose transporter family of Arabidopsis. Proc Natl Acad Sci USA. 2014:**111**(31):11563–11568. https://doi.org/10.1073/pnas.1406073111

Rautengarten C, Heazlewood JL, Ebert B. Profiling cell wall monosaccharides and nucleotide-sugars from plants. Curr Protoc Plant Biol. 2019:**4**(2):e20092. https://doi.org/10.1002/cppb.20092

Rui Y, Anderson CT. Functional analysis of cellulose and xyloglucan in the walls of stomatal guard cells of *Arabidopsis*. Plant Physiol. 2016:**170**(3):1398–1419. https://doi.org/10.1104/pp.15.01066

Sampathkumar A, Gutierrez R, Mcfarlane HE, Bringmann M, Lindeboom J, Emons A-M, Samuels L, Ketelaar T, Ehrhardt DW, Persson S. Patterning and lifetime of plasma membrane-localized cellulose synthase is dependent on actin organization in *Arabidopsis* interphase cells. Plant Physiol. 2013:**162**(2):675–688. https://doi.org/10.1104/pp.113.215277

Schenk S, Hernández-Reyes C, Samans B, Stein E, Neumann C, Schikora M, Reichelt M, Mithöfer A, Becker A, Kogel K-H, et al. N-acyl-homoserine lactone primes plants for cell wall reinforcement and induces resistance to bacterial pathogens via the salicylic acid/oxylipin pathway. Plant Cell. 2014:**26**(6):2708–2723. https://doi.org/10.1105/tpc.114.126763

Schikora A, Schenk ST, Stein E, Molitor A, Zuccaro A, Kogel K-H. N-acyl-homoserine lactone confers resistance toward biotrophic and hemibiotrophic pathogens via altered activation of AtMPK6. Plant Physiol. 2011:**157**(3):1407–1418. https://doi.org/10.1104/pp.111.180604

Schrick K, Debolt S, Bulone V. Deciphering the molecular functions of sterols in cellulose biosynthesis. Front Plant Sci. 2012:**3**:84. https://doi.org/10.3389/fpls.2012.00084

Schrick K, Fujioka S, Takatsuto S, Stierhof Y-D, Stransky H, Yoshida S, Jürgens G. A link between sterol biosynthesis, the cell wall, and cellulose in Arabidopsis. Plant J. 2004:**38**(2):227–243. https://doi.org/10.1111/j.1365-313X.2004.02039.x

Schulze-Lefert P. Knocking on the heaven's wall: pathogenesis of and resistance to biotrophic fungi at the cell wall. Curr Opin Plant Biol. 2004:**7**(4):377–383. https://doi.org/10.1016/j.pbi.2004.05.004

Smith JM, Heese A. Rapid bioassay to measure early reactive oxygen species production in *Arabidopsis* leave tissue in response to living *Pseudomonas syringae*. Plant Methods. 2014:**10**(1):6. https://doi.org/10.1186/1746-4811-10-6

Somerville C. Cellulose synthesis in higher plants. Annu Rev Cell Dev Biol. 2006:**22**(1):53–78. https://doi.org/10.1146/annurev.cellbio.22.022206.160206

Srivastava V, Malm E, Sundqvist G, Bulone V. Quantitative proteomics reveals that plasma membrane microdomains from poplar cell suspension cultures are enriched in markers of signal transduction, molecular transport, and callose biosynthesis. Mol Cell Proteomics. 2013:**12**(12):3874–3885. https://doi.org/10.1074/mcp.M113.029033

Takahashi D, Kawamura Y, Uemura M. Detergent-resistant plasma membrane proteome to elucidate microdomain functions in plant cells. Front Plant Sci. 2013:**4**:27. https://doi.org/10.3389/fpls.2013.00027

Tateno M, Brabham C, Debolt S. Cellulose biosynthesis inhibitors–a multifunctional toolbox. J Exp Bot. 2016:**67**(2):533–542. https://doi.org/10.1093/jxb/erv489

Thiele K, Wanner G, Kindzierski V, Jürgens G, Mayer U, Pachl F, Assaad FF. The timely deposition of callose is essential for cytokinesis in Arabidopsis. Plant J. 2009:**58**(1):13–26. https://doi.org/10.1111/j.1365-313X.2008.03760.x

Tinevez J-Y, Perry N, Schindelin J, Hoopes GM, Reynolds GD, Laplantine E, Bednarek SY, Shorte SL, Eliceiri KW. Trackmate: an open and extensible platform for single-particle tracking. Methods. 2017:**115**:80–90. https://doi.org/10.1016/j.ymeth.2016.09.016

Ton J, Mauch-Mani B. β-amino-butyric acid-induced resistance against necrotrophic pathogens is based on ABA-dependent priming for callose. Plant J. 2004:**38**(1):119–130. https://doi.org/10.1111/j.1365-313X.2004.02028.x

Tran TM, Chng CP, Pu X, Ma Z, Han X, Liu X, Yang L, Huang C, Miao Y. Potentiation of plant defense by bacterial outer membrane vesicles is mediated by membrane nanodomains. Plant Cell. 2022:**34**(1):395–417. https://doi.org/10.1093/plcell/koab276

Tran TM, Ma Z, Triebl A, Nath S, Cheng Y, Gong B-Q, Han X, Wang J, Li J-F, Wenk MR, et al. The bacterial quorum sensing signal DSF hijacks *Arabidopsis thaliana* sterol biosynthesis to suppress plant innate immunity. Life Science Alliance. 2020:**3**(10):e202000720. https://doi.org/10.26508/lsa.202000720

Updegraff DM. Semimicro determination of cellulose inbiological materials. Anal Biochem. 1969:**32**(3):420–424. https://doi.org/10.1016/S0003-2697(69)80009-6

Usadel B, Bläsing OE, Gibon Y, Retzlaff K, Höhne M, Günther M, Stitt M. Global transcript levels respond to small changes of the carbon status during progressive exhaustion of carbohydrates in *Arabidopsis* rosettes. Plant Physiol. 2008:**146**(4):1834–1861. https://doi.org/10.1104/pp.107.115592

Van Kan JA. Licensed to kill: the lifestyle of a necrotrophic plant pathogen. Trends Plant Sci. 2006:**11**(5):247–253. https://doi.org/10.1016/j.tplants.2006.03.005

Verma DPS, Hong Z. Plant callose synthase complexes. Plant Mol Biol. 2001:**47**(6):693–701. https://doi.org/10.1023/A:1013679111111

Xiao S, Chye M-L. Overexpression of Arabidopsis ACBP3 enhances NPR1-dependent plant resistance to *Pseudomonas syringe* pv tomato DC3000. Plant Physiol. 2011:**156**(4):2069–2081. https://doi.org/10.1104/pp.111.176933

Xie B, Wang X, Zhu M, Zhang Z, Hong Z. Cals7 encodes a callose synthase responsible for callose deposition in the phloem. Plant J. 2011:**65**(1):1–14. https://doi.org/10.1111/j.1365-313X.2010.04399.x

Zavaliev R, Levy A, Gera A, Epel BL. Subcellular dynamics and role of Arabidopsis β-1, 3-glucanases in cell-to-cell movement of tobamoviruses. Mol Plant Microbe Interact. 2013:**26**(9):1016–1030. https://doi.org/10.1094/MPMI-03-13-0062-R

Zavaliev R, Ueki S, Epel BL, Citovsky V. Biology of callose (β-1, 3-glucan) turnover at plasmodesmata. Protoplasma. 2011:**248**(1):117–130. https://doi.org/10.1007/s00709-010-0247-0

Zhang Y, Yu J, Wang X, Durachko DM, Zhang S, Cosgrove DJ. Molecular insights into the complex mechanics of plant epidermal cell walls. Science. 2021:**372**(6543):706–711. https://doi.org/10.1126/science.abf2824